Performance Evaluation of IEEE 802.15.4 LR-WPAN for Industrial Applications

Feng Chen*†, Nan Wang†, Reinhard German† and Falko Dressler†
*Siemens AG, Automation and Drives, Germany
†Computer Networks and Communication Systems
Dept. of Computer Sciences, University of Erlangen-Nuremberg, Germany
{feng.chen,german,dressler}@informatik.uni-erlangen.de

***Abstract*—We present a number of performance studies of the IEEE 802.15.4 protocol. We put a special focus on application scenarios in industrial sensor network applications, which is one of the intended application domains for this protocol. The primary requirements are reduced end-to-end latency and energy consumption. Our studies are based on our new implementation of IEEE 802.15.4 developed for the simulation framework OMNeT++. We performed extensive simulations that demonstrate the capabilities of this protocol in the selected scenarios but also the limitations. In particular, we investigated the dependency of the protocol on protocol-inherent parameters such as the beacon order and the superframe order but also to different traffic load. Our results can be used for planning and deploying IEEE 802.15.4 based sensor networks with specific performance demands.**

I. Introduction

IEEE 802.15.4 [1] is a standard designed for low-rate wireless personal area networks (LR-WPAN) and defines the specifications of the physical layer (PHY) and medium access control (MAC) sublayer. In contrast to wireless local area network (WLAN), which is standardized by IEEE 802.11 family, LR-WPAN stresses short-range operation, low-data-rate, energy-efficiency, and low-cost. Thus, LR-WPAN is intended to become an enabling technology for wireless sensor networks (WSNs) [2]. An example is ZigBee [3], which is an open specification built on the LR-WPAN standard and focusing on the establishment and maintenance of LR-WPANs. Such networks are designed for low-rate applications, however they especially stress energy efficiency.

In this paper, we study the applicability of the LR-WPAN techniques in industrial control applications. This application scenario is of special interest because sensor network technology is increasingly demanded in this domain and the IEEE standard provides a protocol developed and accepted in the industry compared to solutions such as S-MAC [4].

Based on the findings by Kohavakka et al. [5] and by Zheng et al. [6], who analyzed the energy aspects of IEEE 802.15.4 in several scenarios, our objective is to extend the performance measurements of the protocol to analyze typical communication parameters such as the packet loss ratio, the end-to-end delay, and the goodput in combination with the energy consumption for specific scenarios relevant to industrial sensor network applications.

The remainder of the paper is organized as follows. In Section II, we give a brief description of IEEE 802.15.4 protocols. Section III introduces the IEEE 802.15.4 model in OMNeT++. The simulation settings and configurations are given in Section IV. In Section V, our simulation results are presented and explained. Finally, Section VI concludes the paper and gives a vision to the future work.

II. A Brief Overview of IEEE 802.15.4

In the following, a brief overview of IEEE 802.15.4 is provided. Only those parts relevant to our performance study are introduced. Readers can refer to [1] and [7] for a more detailed description of the protocol.

The IEEE 802.15.4 network can work in one of three ISM frequency bands and choose from a total of 27 channels. Two different types of devices are defined in an LR-WPAN: a full function device (FFD) and a reduced function device (RFD). An FFD can talk to any other device and serves as a PAN coordinator, a coordinator, or a device. An RFD can only talk to an FFD node. Furthermore, the standard supports two network topologies: star and peer-to-peer. In star networks, the communication occurs only between devices and a single central controller, called the PAN coordinator, which manages the entire PAN. The peer-to-peer topology also has a PAN coordinator, however it differs from the star topology as any of the devices can arbitrarily communicate with each other as long as they are within a common communication range. A special case of peer-to-peer topology is cluster tree, in which a node talks only to its parent or children nodes. For a more detailed description of the possible topologies, please also refer to [5].

In order to achieve better energy-efficiency, IEEE 802.15.4 can operate in a so called *beacon-enabled* mode, for which a superframe structure is utilized as shown in Figure 1. A *superframe* is bounded by periodically transmitted beacon frames, which allow nodes to associate with and synchronize to their coordinator. Each superframe consists of two parts: an active and an inactive period. The length of the beacon interval (BI) and the active period, which is also referred to as superframe duration (SD), are determined by two parameters: the beacon order (BO) and the superframe order (SO), respectively. Their calculations are shown in Figure 1. *aBaseSuperframeDuration* equals to 960 symbols. To use the superframe structure, PANs shall set BO to a value between 0 and 14 and SO to a value

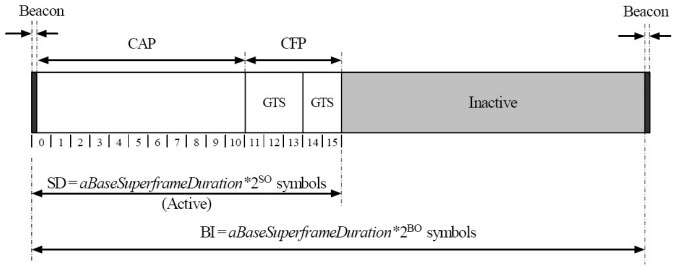

Fig. 1. Superframe structure in a beacon-enabled PAN

between 0 and the value of BO, which results in the range of BI and SD between 15.36 ms and 251.7 s at the 2.4GHz band. The active portion is further divided into 16 contiguous time slots that form three parts: the beacon, the contention access period (CAP), and the contention-free period (CFP). In CAP, all data transmissions should follow a successful execution of the slotted CSMA-CA algorithm. There are two data transfer modes defined in CAP, the indirect transmission for downlink data and the direct transmission for uplink data. In CFP, a device can communicate with the PAN coordinator directly in so called guaranteed time slots (GTS) without contending for the channel using CSMA-CA mechanism. The GTSs are allocated by the PAN coordinator, therefore the GTS transfer mode is only applicable in star networks.

III. LR-WPAN Model in OMNeT++

We first present a simulation model of LR-WPAN in OMNeT++ [8]. OMNeT++ is a public-source, component-based and discrete event simulation environment and is becoming very popular especially in communications and networking community. Its primary application area covers the simulation of communication networks. Nevertheless, other types of event based simulation are addressed as well including systems and business processes.

Our model of IEEE 802.15.4, which is based on the ns-2 implementation [6], has been developed using the INET framework, which is an open-source communication networks simulation package for OMNeT++ and suited for simulations of different kinds of wired and wireless networks. A great number of protocols are already available in this framework. The structure and components of the LR-WPAN model are shown in Figure 2. The model consists of an 802.15.4 based protocol stack and two protocol-independent modules supporting energy measurement and mobility in the simulations. A screen snapshot of the model in the graphical interface of OMNeT++ is shown in Figure 3. In the following, we briefly introduce the functionality of each module. More detailed introduction of the model can be found in [9].

A. LR-WPAN Protocol Stack Model

The model for the LR-WPAN protocol stack has four layers plus an interface queue (IFQ) module that acts as the buffer of the MAC layer. The MAC and PHY modules are the core of the implementation and modeled strictly conforming to the

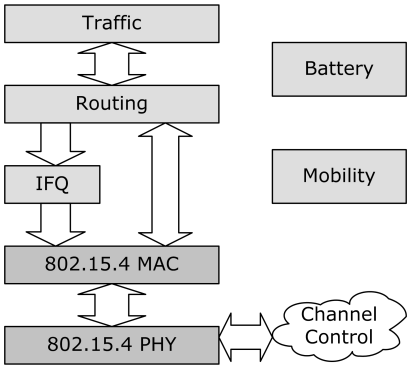

Fig. 2. The structure and components of the LR-WPAN model in OMNeT++

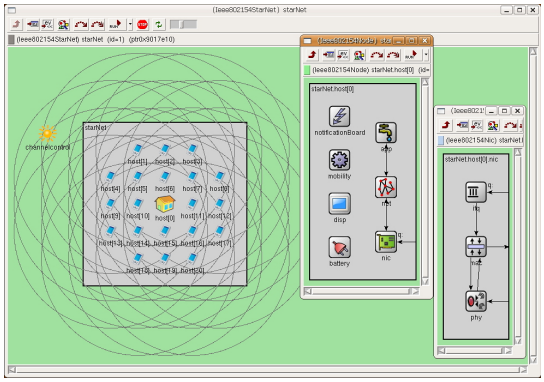

Fig. 3. The screen snapshot of the LR-WPAN model in OMNeT++

IEEE standard 802.15.4-2006. The following PHY functions defined in the specifications have been implemented:

- Radio implemented in both a three-switch-state model (*receiver-on, transmitter-on, turnoff*) facilitating implementation of MAC-PHY primitives and a four-work-state model (*idle, sleep, receiving, and transmitting*) for the purpose of energy measurement and carrier sensing
- Packets transmission/reception with collision detection
- Energy detection (ED) and clear channel access (CCA)
- Ideal/lossy channel supporting channel switch

For the purpose of our study, we have concentrated on modeling the data transfer related functions of the MAC layer. As for PAN formation and management functions defined in the MAC specification, only a simplified association process has been implemented. In addition, security related specifications [10] are not yet considered in our model. Even though we did not mean to build a complete IEEE 802.15.4 model, the code size for the MAC and PHY still reaches approximately 7000 lines of code. The following MAC functions defined in the specifications have been implemented:

- Both slotted and unslotted CSMA-CA
- Both beaconed and non-beaconed mode
- Direct, indirect, and GTS data transfer models
- Interframe spacing (IFS), frame filtering and duplication detection
- Association with coordinators

Above the MAC layer, we explicitly added three modules, which are outside the scope of the LR-WPAN specifications. The IFQ module is in fact a drop-tail FIFO queue, which buffers data packets coming from the upper layer and feeds them to the MAC upon request. The maximum queue length (buffer size) is adjustable. The routing module is built to forward packets in star and cluster-tree topologies as well as to support the formation of cluster-tree PANs. The traffic module plays the role of packet generator at source nodes or the role of packet collector consuming these packets at sink nodes. Using a flexible XML-based parameter structure, it can be configured to generate various types of traffic, including the usual constant bit rate (CBR), on-off, and exponentially distributed traffic.

B. Battery and Mobility Modules

The analysis of the energy performance is one of the main objectives of our study. To measure the energy consumed by radios at sensor nodes, we implemented a battery model in OMNeT++. By tracking the current radio state in the PHY module, the battery module counts the total time that the radio has spent in each of the four working states and calculates the corresponding energy consumption using the given radio power values. Our battery model provides real-time calculation of energy consumption and can display the remaining energy level for each node in the animation. In addition, it can easily be adapted for evaluation of the network lifetime as a primary result of our simulations. For example, when a certain node in the network has exhausted its battery, we can let it stop communicating with other active nodes and keep running the simulation until all nodes in the network die. Our model currently relies on energy measurements for the CC1000 radio on Mica2 motes [11]. Nevertheless, it can easily be updated to any other hardware, e.g. the CC2420 radio specially designed for IEEE 802.15.4, if exact measurements are provided.

The mobility module supports simulating static or dynamic topologies. For static simulations, nodes can be placed at a fixed position or be spread randomly within a specified area. The random placement is useful in simulations that evaluate the formation of cluster-tree networks for application in sensor networks.

IV. Simulation Settings

We describe in this section the configuration and settings of the LR-WPAN model in OMNeT++ for our performance study, including parameter settings and definition of performance measures.

As mentioned in the previous section, star networks have advantages compared to mesh networks in terms of robustness and latency. These two aspects are often put into first consideration in many industrial control applications. Sensor networks are still being evaluated for applications in automation processes. IEEE 802.15.4 is a perfect candidate for these environment due to various reasons including the available industry standard. Objectives are usually a high reliability of the communication, energy efficiency, and low latency.

TABLE I
Model Parameters

PHY Module Parameters	
Channel number, bitrate	11, 250 kb/s
Transmitter power	1 mW
Transmission range	172 m
Carrier sense sensitivity	-85 dBm
MAC and IFQ Module Parameters	
Synchronization mode	beacon-enabled
Topology type	star
Data transfer model	direct with ACK enabled
IFQ size (buffer)	1
Traffic Module Parameters	
Traffic type	exponential
Payload size	50 bytes
Battery Module Parameters	
Radio power in sleeping	0.06 mA
Radio power in idle	1.38 mA
Radio power in receiving	9.6 mA
Radio power in sending	17 mA

Therefore, we focus in this paper on IEEE 802.15.4 based star networks. Energy consumption is one of the most important considerations in choosing or designing sensor networks for industrial applications. The beaconing synchronization mechanism in IEEE 802.15.4 enables networks to work under a controllable duty cycle to achieve better energy efficiency compared to the non-beacon mode. Therefore, the beacon-enabled mode has been chosen in all our simulations. In Table I, some important model parameters fixed throughout our study are listed. Other internal protocol parameters use default values specified in the IEEE standard. Variable parameters together with scenarios and corresponding results will be introduced in the next section.

The performance of IEEE 802.15.4 based star networks for industrial applications is evaluated in terms of two aspects, energy performance and end-to-end communication performance. One energy measure and three end-to-end measures have been used as described in the following:

- *Energy consumption per payload byte* – the average energy consumed for successfully transmitting one payload byte from the source to the sink by the whole network
- *End-to-end packet loss rate (PLR)* – the ratio of the number of packets dropped by the network (both at IFQ due to queue overflow and at MAC due to exceeding maximum retries) to the total number of packets generated at the source nodes
- *End-to-end delay* – the average delay for a single packet from source to sink
- *End-to-end goodput* – the average number of payload bytes received at the sink node per time unit

In all our experiments, statistical significance of the simulation results has been carefully considered. For every simulation with the same input parameters, we run five independent replications, from which the mean value is calculated for each performance measure and plotted as a single point in the graph. The simulation time required for each simulation varies drastically with the input traffic and parameter settings,

however, it has been chosen long enough to guarantee that more than 5000 packets are received by the sink at the end of each running. The simulation results were plotted in the form of linespoints without errorbar, because the maximum relative standard deviation of the results is less than 1%, which could be unobservable on the graphs.

V. Simulation Results

The previous section described the common settings for our simulations. In this section, the simulation results from two selected scenarios are presented and discussed. In particular, we analyzed a 3 node scenario and a 21 node scenario as described in the following.

A. First Scenario: 3 Nodes, 50% Duty Cycle

In the first scenario, we studied a star network with one PAN coordinator and two devices. These three nodes are placed in a row, with the PAN coordinator located in the middle of the other two nodes. To introduce the hidden terminal problem, the distance between the two outer devices is 200 meters, which exceeds the preset radio transmission range of 172 meters as listed in Table I. One device is attached with an exponential traffic source and sends packets via the PAN coordinator to the other device. The duty cycle is set to 50% in all the nodes, however, configured with various combination of BO and SO.

For schedule-based MAC protocols such as IEEE 802.15.4, which defines a superframe structure with periodic active and sleeping periods, it is assumed that the duty cycle should determine the level of the overall energy consumption. We intended to validate this assumption in our simulations. In addition, we were also interested to see how the end-to-end performance of the studied network will be affected by various parameter configurations (mainly BO and SO) and traffic conditions with constant duty cycle. The simulation results are plotted on graphs for each performance measure. Due to a wide variation range in the measured values, logarithmic scaling has been applied on the vertical axis on all the graphs for this scenario exclusive of that for PLR.

Figure 4(a) shows the measured mean energy consumption for transmitting one payload byte plotted on a logarithmic scale. As expected beforehand, under the same duty cycle, energy consumption shows to be less sensitive to the parameter combination than to the traffic load. For the same (BO,SO), the energy consumption decreases with increasing traffic load, because the average number of transmitted packets per beacon interval increases rapidly – this can be also observed in the goodput graph as shown in Figure 4(d). However, the energy consumption per beacon interval does not increase as significantly as the number of sent packets does, because the increased energy consumed for transmitting more packets does not increase the overall energy consumption per beacon too much in the case of the same duty cycle. It can be also observed that when the traffic load is light relative to a certain combination, energy consumption increases approximately linearly with packet generating interval. For example, the traffic load is relatively light at the top three points under the combination of (1,0), which can be proved at the corresponding points with very low PLR values on the PLR graph as shown in Figure 4(b).

Another trend revealed by each single curve on the energy graph is that under the same traffic load, the network needs more energy to transmit one payload byte when configured with a larger combination of BO and SO. This is especially obvious for the mean message interval of 0.01 s curve, which is the highest one among all the traffic loads. In fact for the same traffic load, the relative traffic condition becomes heavier as the length of BI increases while the duty cycle keeps constant. This can be proved by the increasing PLR as shown in the PLR graph in Figure 4(b). Since the packet interval is the same for one curve, the higher PLR means that less packets have been received per time unit, which is clearly shown in the goodput graph in Figure 4(d). However, the mean energy consumption per time unit will remain approximately the same independent of the values of BO and SO, because the node is always busy sending or receiving packets while the PLR is not low and the duty cycle dominates the overall energy consumption. Therefore, it can be concluded from the above analysis that when averaged to each transmitted payload byte, the mean energy consumption will increase with the values of BO and SO.

Figure 4(b) shows the measured end-to-end PLR, which reveals the capacity of the network under various parameter settings. For the same (BO,SO), the PLR increases with the traffic load, which is self-explaining. The reason for each curve ascending as the BI becomes longer is due to the increasing relative traffic load, which has been explained previously. Comparing all the curves in the graph, we can notice that the PLR curve rises earlier under higher packet generating rate, which is the combination result of the previous two rules. It can be observed from the PLR graph that the (1,0) combination has the largest capacity.

Figure 4(c) depicts the measured mean end-to-end delay on a logarithmic scale. For the small (BO,SO) as shown on the left-hand side of the graph, the delay stays at a very low level, independent of the applied traffic load. The reason is that all the traffic conditions are relatively light at the small (BO,SO) values. Most packets can be transmitted successfully from the source to the sink with a high delivery rate and very few packets suffer from long waiting time in the queue due to contending for the channel or going through the sleeping period. We can notice that at (1,0), the delay under the load of 0.01 s is a little higher than that under the other traffic conditions. This can be explained by the higher loss rate as shown in the PLR graph due to the higher traffic load. In this case more packets have to wait in the queue for the next active period at the intermediate node before they can be forwarded to the sink. Since the sleeping period is only about 15 ms when SO=0, the extra queue delay will not significantly increase the overall mean delay. When the the values of (BO,SO) increase, the delay curve ascends because of the increased inactive period, which introduces longer queue delay.

Another interesting phenomenon in the delay measurements

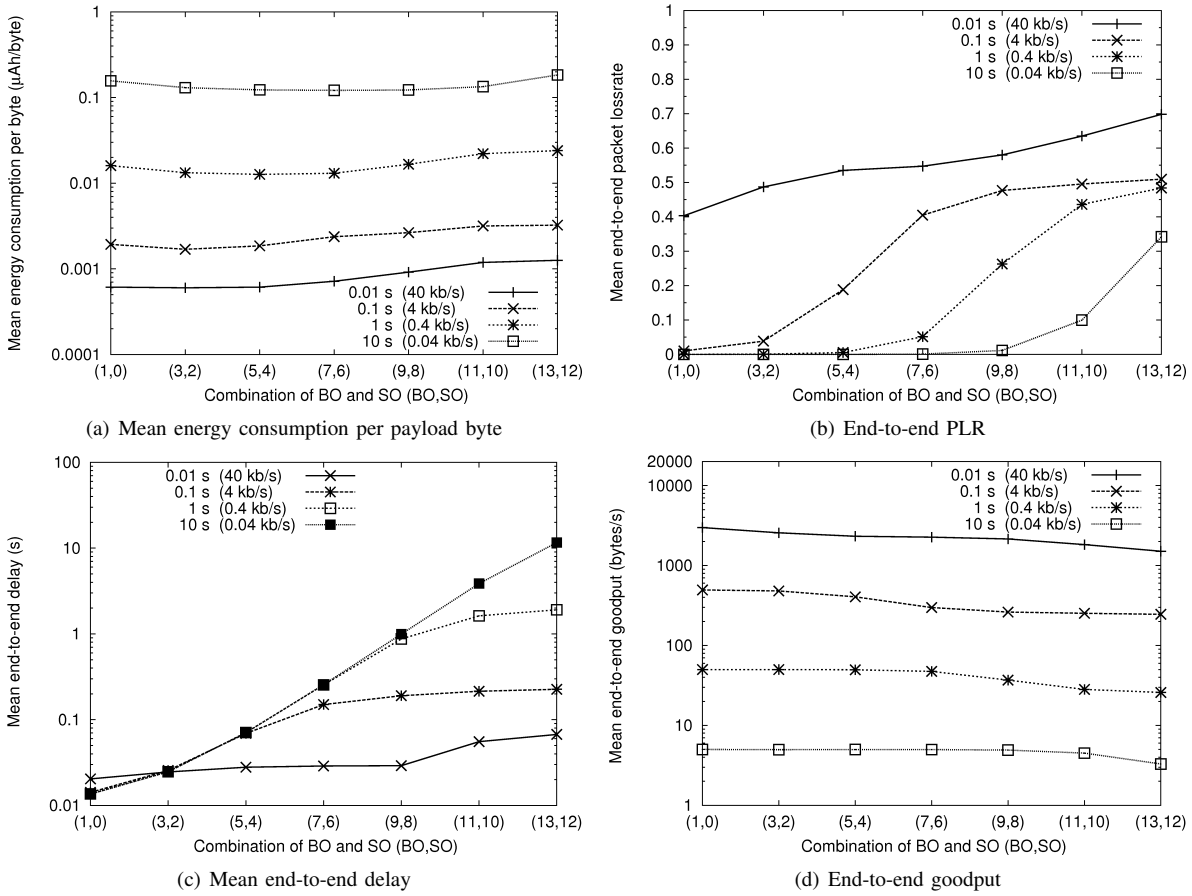

(a) Mean energy consumption per payload byte

(b) End-to-end PLR

(c) Mean end-to-end delay

(d) End-to-end goodput

Fig. 4. Energy and end-to-end performance for different combination of BO and SO with 50% duty cycle under exponential traffic load

can be observed for the (BO,SO) combination of (13,12) on the right-hand side of the graph. The mean delay for the packet interval of 10 s is about 10 s, which is three orders of magnitude bigger than the mean delay for the packet interval of 0.01 s. Such huge difference is mainly caused by the long BI and SD, which equal to 126 s and 63 s, respectively, for the (BO,SO) combination of (13,12). Because the length of active period is much longer than the packet interval in all the traffic conditions, the number of transmitted packets per BI will increase approximately linearly with the number of packets generated per BI, which can be proved by the goodput graph shown in Figure 4(d). Within a beacon interval, since the IFQ size is set to 1, at most two packets (one in the IFQ and one at MAC) will suffer from a fairly long delay due to the long inactive period of 63 s at (13,12). In general, the overall mean end-to-end delay in this case is determined to a certain extent by the number of those packets, which are sent immediately within a beacon interval without experiencing a long inactive period. Therefore, the much smaller delay at the higher traffic load is contributed by the large amount of small delays per BI that have largely averaged a few extremely large delays to a small value.

Figure 4(d) shows the measured end-to-end goodput on a logarithmic scale. Compared with those in the energy graph as shown in Figure 4(a), the curves for goodput show a similar but inverse trend. Under the same duty cycle, the goodput is mainly determined by the traffic load and shows less dependency on the other parameters. According to the queuing, when the traffic is very light and no packets get lost in the network, the number of packets outgoing per time unit should be equal to the number of packets arriving per time unit. In the goodput graph, this theory applies at those points that are corresponding to about zero loss in the PLR graph, which partially validates our simulation results. Under the same traffic load, the goodput decreases with the increase of the (BO,SO) due to the rising PLR, which has been explained previously.

B. Second Scenario: 21 Nodes, effects of BO and SO

In the previous section, we investigated the performance of a three-node star network by exploring various (BO,SO) combinations of 50% duty cycle, which is regarded as a starting point of our study. Now, we simulate a larger star network, which models a typical applicaiton using WSN techniques in industrial control fields. The scenario can be described as follows: 20 devices equipped with various sensors are scattered within an area and associated to a central node, the PAN coordinator, to form a monitoring or control network. Upon detecting that single readings exceed a predefined threshold,

related information must be sent to the PAN coordinator within a well-specified time. For such applications, low-latency is usually put in the first place, while energy efficiency is also another important consideration. Since one of these two aspects is usually achieved by sacrificing the other on performance, simuations can help us to find out a proper balance point for a certain requirement.

The topology of this scenario has been shown previously in Figure 3. 20 devices are placed symmetrically around the PAN coordinator with an equal distance of 30 meters to each of their neighbors. Communications only occur between the devices and the PAN coordinator. Each device sends packets generated by its own exponential traffic source to the PAN coordinator. The packet generating interval is varied between 0.01 s and 100 s. Due to large range of the packet interval, logarithmic scaling has been used on the horizontal axis on all the graphs. For similar reasons, logarithmic scaling has been also applied on the vertical axis on all the graphs except for that for PLR.

In the first set of experiments, we fixed SO to 2 and study the effect of various BO at 3, 5, 7, and 9, which correspond to a duty cycle of 50%, 12.5%, 3.125%, and 0.781% respectively. Figure 5(a) shows the measured mean end-to-end PLR. Similar to the first scenario, packet loss occurs either due to IFQ overflow or due to exceeding the maximum number of reransmissions caused by collisions. With decreasing traffic load, the PLR descends from the top value of near 100% gradually down to a small value close to zero. The curve with a smaller BO starts to decline earlier, showing the stronger capacity due to its higher duty cycle. Because we configured the IFQ to 1, as long as the queue is full, i.e. for higher traffic rates, collisions will exist. Thus, the PLR is caused by two effects: tail drop at the IFQ (dominating at higher traffic rates) and collisions in the MAC (dominating at lower traffic rates).

The measured mean energy consumption per payload byte is depicted in Figure 5(b). In the area of heavy traffic load on the left-hand side of the graph, the energy consumption under the same traffic load increases with the increasing length of BI. For example for a traffic interval of 0.01 s, due to the same length of the active period, the average number of packets transmitted per BI are almost the same for various SO. This means that almost the same amount of energy is consumed in the active period. Therefore, the longer BI consuming more energy is caused by more energy consumption in the inactive period. Under heavy traffic, the energy consumption on each curve remains constant independent of the traffic load, because the MAC is almost fully loaded. The total energy consumed in the active period has reached its peak value and the number of transmitted packets per BI is saturated, which can be seen in the goodput graph. Therefore, the total energy averaged to each payload byte is constant. As the traffic load keeps decreasing, the energy curve drops first and then ascends monotonously. The drop in energy consumption is contributed by the decrease in the number of collisions per BI, which reduces the energy wasted in resending. The starting point for descending on the energy graph is right the turning point at which the PLR at the IFQ has dropped to a low level and the PLR at the MAC starting to decrease, as mentioned previously. When the collision rate has bottomed out, the energy consumption reaches its minimum value at this point. The increasing trend in energy consumption on the right-hand side of the graph can be explained as follows. As the traffic load gets lighter, less packets are transmitted per BI and the ratio of energy consumed on idle listening increases. When idle listening starts to contribute to the most percentage of the overall energy consumption, the mean energy consumption per payload byte will increase inverse proportionally to the packet generating rate. In the area of energy ascending on all the curves, the smallest BO consumes the most energy, because with the same SO higher duty cycle under light traffic means more energy consumption per unit time. However, the number of packets transmitted per time unit are almost the same, which can also be explained on the goodput graph as shown in Figure 5(d).

Figure 5(c) shows the measured mean end-to-end delay on a logarithmic scale. At the same packet interval, the smaller BO with the same SO achieves lower latency benefiting from its shorter inactive period, in which the buffered packets may experience a relatively long delay. In the case of very light traffic load, the end-to-end delay remains at its theoretic minimum value, which is contributed mainly by random backoff delay, transmission delay and sleeping delay and suffers little from delays in queuing, additional backoffs or retransmission. As the traffic load increases, the end-to-end delay rises due to the increasingly intense contention on the channel and the rising number of collisions. However, as the traffic load gets heavier and heavier, the delay will not keep rising but stay at a saturation value, because the MAC reaches its maximum ability and most packets are dropped at the IFQ.

Figure 5(d) shows the measured mean end-to-end goodput. Under high traffic load, the smaller BO resulting in higher duty cycle can achieve much better bandwidth utilization and, therefore, much higher goodput. As the traffic load goes lighter, the goodput will reach its peak value at the same point on the traffic load axis as on the energy graph, where the minimum energy consumption per byte is achieved because the collision rate has reached minimum while the channel is still fully utilized at a critical point. As the traffic load keeps decreasing, the goodput curve goes down monotonously, the level of which is determined by the packet generating rate. When the traffic load is low enough, for example at the interval of 100 seconds, the goodput becomes parameter-independent within a certain variation range of BO, because the packet interval is much longer than the BI in all the cases and the goodput is basically the same with the packet inter-arrival rate.

In a second set of experiments, we fixed BO to 8 and study the effect of various SO at 0, 1, 3, 5, and 7. The simulation results are depicted in Figure 6. The obtained results underline the effects described for the previous measurement (fixed SO). The modification of SO leads to different proportions of the active period compared to the inactive period. Thus, the PLR curves for small SO are higher as depicted in Figure 6(a). This is due to the small active period in which only a few packets

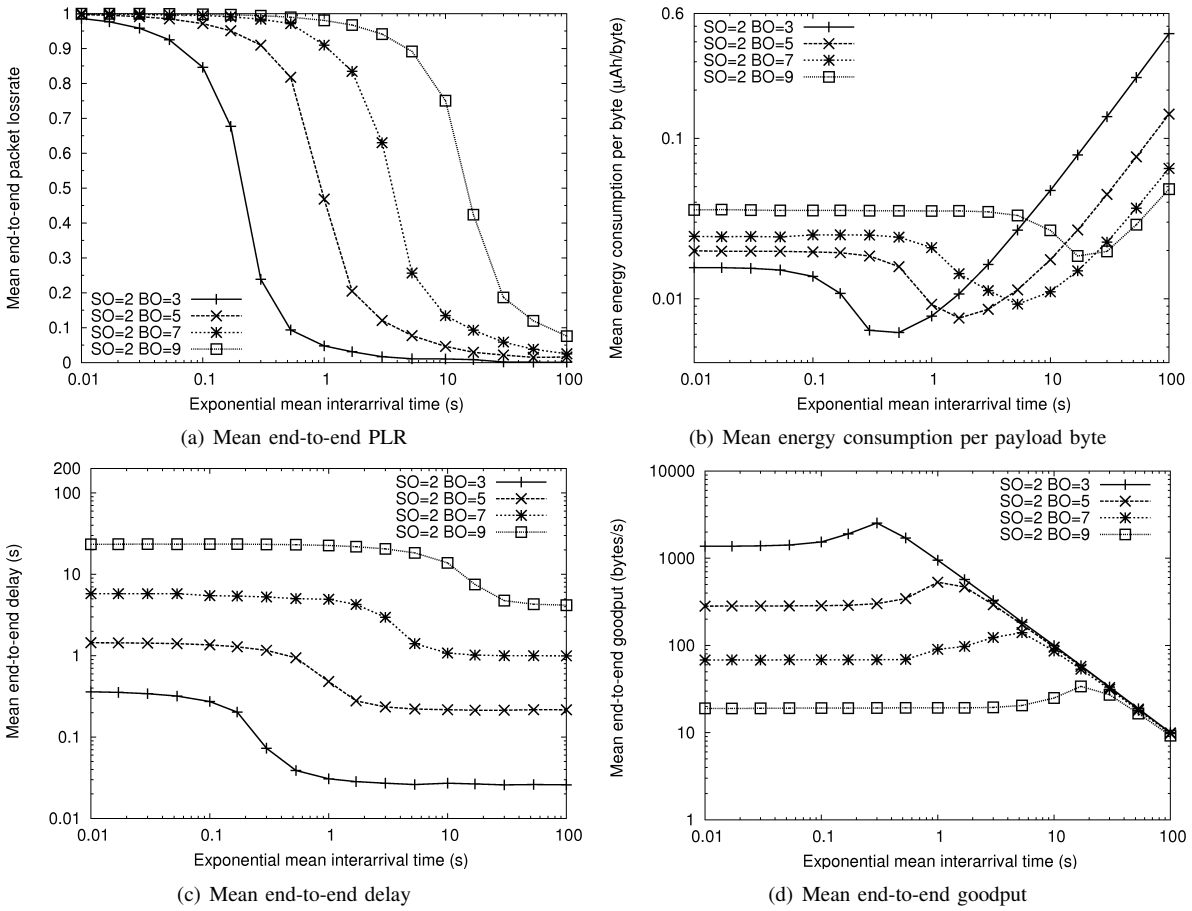

(a) Mean end-to-end PLR

(b) Mean energy consumption per payload byte

(c) Mean end-to-end delay

(d) Mean end-to-end goodput

Fig. 5. Energy and end-to-end performance for SO=2 and various values of BO under exponential traffic load

can be transmitted. This effect can also be seen in the delay curves shown in Figure 6(c).

For high traffic rates, almost all packets are dropped by the IFQ. Thus, the goodput will remain constant until the traffic rate drops below a value at which the network is able to handle the load. In Figure 6(d), this effect is shown. After passing this specific traffic rate, the measured goodput converges to the traffic rate for all values of SO. This trend is slower for small SO because the inactive period is much smaller for this parameter setting.

Finally, the energy measurements shown in Figure 6(b) need to be discussed. Interestingly, the consumed energy decreases for decreasing SO (7 down to 3) but increases again for further decreasing values of SO (1 and 0) and high traffic rates. This effect can be explained as follows. The energy model of the sensor consumes energy not only for transmitting packets but also for the inactive period. For a small SO equal to 0, the inactive period is about 1,000 times larger than the active period. Thus, the energy consumption for sitting idle dominates. We executed further simulations with a recalibrated energy model (no energy is consumed in the inactive period) and figured out that the energy curves for decreasing values for SO are shaped similar to the higher values (these have been discussed for constant SO before).

To sum up the above performance analysis, each curve in the graphs shown in Figures 5 and 6 can be divided into three areas according to the degree of the relative traffic load, which include the areas for heavy traffic, moderate traffic, and light traffic. In the heavy traffic area, the higher duty cycle under the same SO can achieve better performance in both the energy consumption and the end-to-end aspects. This rule will still apply when the traffic load decreases from high to moderate. Under very light traffic, which is usually the case in most sensor network applications, especially in our studied scenario aiming at industrial applications, higher duty cycle achieves lower latency at the cost of more energy consumption. Such a trade-off between energy efficiency and low-latency can be optimized through carefully choosing the combination of the parameters BO and SO, which dominate the overall performance, according to the requirements by the specific applications. Our performance study based on a typical industrial application has revealed the complex relation among energy consumption, end-to-end performance, parameter configurations and traffic loads. The simulation results can support such optimization problems.

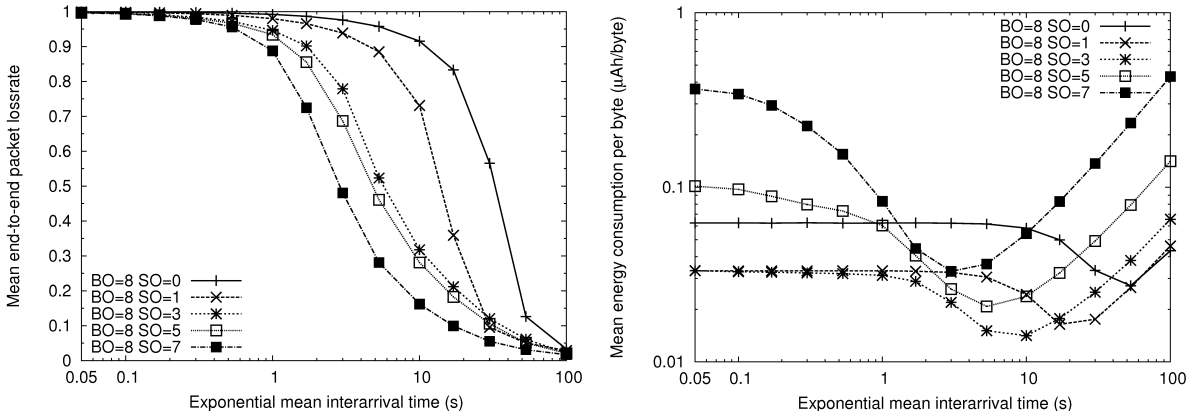

(a) Mean end-to-end PLR

(b) Mean energy consumption per payload byte

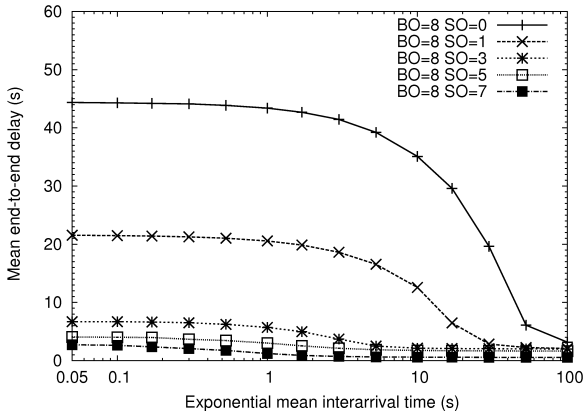

(c) Mean end-to-end delay

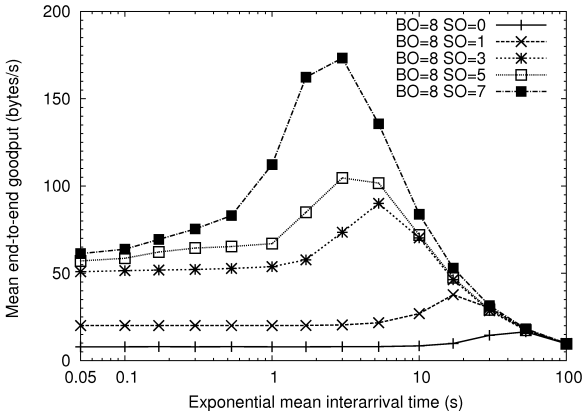

(d) Mean end-to-end goodput

Fig. 6. Energy and end-to-end performance for BO=8 and various values of SO under exponential traffic load

VI. Conclusion and Future Work

We conducted a simulative performance study of LR-WPAN based on our simulation model that has been implemented for OMNeT++. We analyzed two different scenarios, one with a small three-node star topology and the other with a 21-nodes star network modeling a typical industrial sensor network application. The simulation results for one energy measure and three end-to-end measures were analyzed in detail, which can be used to support the parameter configuration and optimization in IEEE 802.15.4 based sensor networks. In future work, we will continue to study the applicability of IEEE 802.15.4 in low-latency and energy-aware applications especially in industrial control fields. More simulations using a wider range of protocol parameters will be run for more complex topologies. Based on our findings, we are working on improved versions of the protocol for application in various scenarios focusing on low-energy consumption with strict quality of service constraints such as delay bounds.

References

[1] IEEE, "Wireless Medium Access Control (MAC) and Physical Layer (PHY) Specifications for Low Rate Wireless Personal Area Networks (WPANs)," IEEE Sandard 802.15.4-2006, 2006.

[2] I. F. Akyildiz, W. Su, Y. Sankarasubramaniam, and E. Cayirci, "Wireless sensor networks: a survey," *Elsevier Computer Networks*, vol. 38, pp. 393–422, 2002.

[3] ZigBee Alliance homepage. [online]. available: http://www.zigbee.org.

[4] W. Ye, J. Heidemann, and D. Estrin, "An Energy-Efficient MAC Protocol for Wireless Sensor Networks," in *21st IEEE Conference on Computer Communications (IEEE INFOCOM 2002)*, vol. 3, New York, NY, USA, June 2002, pp. 1567–1576.

[5] M. Kohvakka, M. Kuorilehto, M. Hännikäinen, and T. D. Hämäläinen, "Performance Analysis of IEEE 802.15.4 and ZigBee for Large-Scale Wireless Sensor Network Applications," in *3rd ACM International Workshop on Performance Evaluation of Wireless Ad Hoc, Sensor, and Ubiquitous Networks (ACM PE-WASUN 2001)*, Terromolinos, Spain, 2006, pp. 48–57.

[6] J. Zheng and M. J. Lee, "A comprehensive performance study of IEEE 802.15.4," in *Sensor Network Operations*. IEEE Press, 2006, pp. 218–237.

[7] ——, "Will IEEE 802.15.4 Make Ubiquitous Networking a Reality?: A Discussion on a Potential Low Power, Low Bit Rate Standard," *IEEE Communications Magazine*, vol. 42, no. 6, pp. 140–146, June 2004.

[8] A. Varga, "The OMNeT++ Discrete Event Simulation System," in *European Simulation Multiconference (ESM 2001)*, Prague, Czech Republic, 2001.

[9] F. Chen and F. Dressler, "A Simulation Model of IEEE 802.15.4 in OMNeT++," in *6. GI/ITG KuVS Fachgespräch Drahtlose Sensornetze, Poster Session*, Aachen, Germany, July 2007, pp. 35–38.

[10] V. B. Misic, J. Fung, and J. Misic, "MAC Layer Security of 802.15.4-Compliant Networks," in *2nd IEEE International Conference on Mobile Ad Hoc and Sensor Systems (IEEE MASS 2005): International Workshop on Wireless and Sensor Networks Security (WSNS'05)*, Washington, DC, USA, November 2005.

[11] O. Landsiedel, K. Wehrle, and S. Gtz, "Accurate Prediction of Power Consumption in Sensor Networks," in *Second IEEE Workshop on Embedded Networked Sensors (EmNetS-II)*, Sydney, Australia, May 2005.